Aerosol and Air Quality Research, 18: 1118–1130, 2018

ISSN: 1680-8584 print / 2071-1409 online
doi: 10.4209/aaqr.2017.11.0471

Design and Performance Evaluation of a Laboratory-made 200 nm Precut Electrical Cascade Impactor

Jangseop Han[1+], Joohee Seo[1+], Dongho Park[2], Junho Hyun[3], Jungho Hwang[1,3*]

[1] *Department of Mechanical Engineering, Yonsei University, Seoul 03722, Korea*
[2] *Department Korea Institute of Industrial Technology (KITECH), Chungcheongnam-do 31056, Korea*
[3] *Graduate program of Clean Technology, Yonsei University, Seoul 03722, Korea*

ABSTRACT

Increasing public concern regarding air quality has led to the development of efficient aerosol-monitoring techniques. Among the various aerosol measurement instruments based on electrical methods, in this study, an electrical cascade impactor (ECI) was designed and fabricated in our laboratory and was used to measure the real-time size distribution of submicron-sized aerosols. In the study by Park *et al.* (2007), it was assumed that the size distribution of incoming particles follows a unimodal lognormal distribution. However, in this study, the distribution of particles captured at each stage (including the Faraday cage) was assumed to be a unimodal lognormal distribution; hence, the incoming particles may follow any size distribution. After the particle charging characteristics were obtained for different particle sizes, experiments were performed with monodisperse test particles to determine the collection efficiency of each stage. The current measured in each stage was converted into a number based size distribution of aerosols by using the data inversion algorithm, which utilized the experimentally obtained collection efficiency. Then, a performance evaluation was performed, both in the laboratory and in the field. The results obtained by our ECI were in agreement with the scanning mobility particle sizer (SMPS) data.

Keywords: Electrical cascade impactor; Submicron-sized aerosols; Corona charger; Data inversion algorithm; Particle size distribution.

INTRODUCTION

Increasing public concern regarding air quality has led to the development of efficient aerosol-monitoring techniques. The real-time aerosol number concentration can be measured by using optical and electrical methods. The optical method typically uses light-scattering technology. However, for particles smaller than approximately 0.3 μm, the light-scattering intensity drops very rapidly. Among the various aerosol measurement instruments based on electrical methods, the Electrical Low Pressure Impactor (ELPI), which has been manufactured and distributed by Dekati Ltd. since 1995, enables real-time (1 s) detection of particles by combining electrical detection of charged particles with a 12-stage low-pressure cascade impactor for measurements of particles smaller than 10 μm (Keskinen *et al.*, 1992; Marjamäki *et al.*, 2000). Yli-Ojanperä *et al.* (2010) improved the nanoparticle resolution of ELPI by designing and manufacturing a new impactor stage for the impactor. The performance of the new impactor construction was evaluated with laboratory and heavy duty diesel exhaust measurements. For nanoparticles, the resolution and precision were improved with the new construction.

Numerous epidemiologic and toxicological studies have suggested that exposure to $PM_{2.5}$ leads to adverse health effects, particularly cardiovascular and respiratory diseases, as well as pre-mature death (Pope and Dockery, 2006; USEPA, 2009; Jiang *et al.*, 2018). $PM_{2.5}$ is deposited throughout human respiratory tract, causing lung diseases, heart diseases, and premature death. Moreover, the biological potency of ultrafine particles (UFPs), which have aerodynamic sizes smaller than 100 nm, increases depending on the content of redox cycling organic chemicals and their ability to damage mitochondria (Ning *et al.*, 2003). UFPs are mainly derived from combustion sources and contain organic carbon compounds such as polycyclic aromatic hydrocarbons (PAHs), which are capable of inducing oxidative stress in macrophages and bronchial epithelial cells. According to the physical and chemical properties of UFPs given by Ning *et al.* (2008), it is very likely that

[+] These authors are equally contributed.

[*] Corresponding author.
Tel: 82-2-2123-2821; Fax: 82-2-312-2821
E-mail address: hwangjh@yonsei.ac.kr

these particles are more dangerous than larger sized particles from the perspective of oxidant injury and inflammation.

In this study, a laboratory-made electrical cascade impactor (ECI) is introduced. The ECI has 5 impactor stages: one is the pre-cut stage, which captures particles larger than 250 nm in aerodynamic diameter, and the others are for measuring particles of size 150 nm–30 nm. There is a filter stage to measure particles of size 30 nm–10 nm. Instead of using a pin-to-plate type corona charger, which is used in ELPI, a wire-to-rod type corona charger serves as the particle charger for the ECI, since it has been reported that in pin (needle) type corona devices, the usage of a pin can wear the pin out and change its geometry, leading to a change in charging efficiency levels. The usage of a pin can also promote the formation of new particles, either from erosion and sputtering from the pin itself or from gaseous contaminants present in the gas (Alonso *et al.*, 2006; Kleefsman and van Gulijk, 2008; Domat *et al.*, 2014).

In one of our previous works (Park *et al.*, 2009), a 4-stage electrical low pressure impactor was designed. After evaluating the collection efficiency of each stage of the impactor, the size distributions of the test particles (sodium chloride (NaCl) particles and DOS particles) were estimated using electrical current data and an inversion algorithm with an assumption of unimodal lognormal distribution (Park *et al.*, 2007). The estimated size distributions were found to agree with the results obtained by a scanning mobility particle sizer (SMPS). Then, the 4-stage electrical low pressure impactor was used to measure the size distribution of diesel particulate matter (< 1 μm) in less than 5 s.

In this study, the data inversion algorithm of Park *et al.* (2007) is modified so that particle sizes having a multimodal lognormal distribution can be measured. In the ECI, the charging efficiency of the charger is represented as $P{\cdot}n$ value, where P is the penetration of particles passing through the charger and n is the average charge number. After the $P{\cdot}n$ values of the particles are obtained for different particle sizes, experiments are performed with monodisperse test particles to determine the collection efficiency of each stage. The current measured in each stage is converted into the number based size distribution of aerosols by using a data inversion algorithm, which utilizes the experimentally obtained collection efficiency.

DESIGN

The corona charger consists of a ceramic body (width of 10 mm, height of 13 mm, and length of 20 mm), a 40 μm-diameter wire as the discharge electrode, and a pair of 1.5 mm-diameter rods as the ground electrode. A structure diagram of the corona charger is provided in Supplemental Information.

In the corona charger, the ion concentration, N_{ion}, is estimated by using the following equation:

$$N_{ion} = \frac{I_C}{eZ_{ion}EA} \tag{1}$$

where I_c is the corona current, Z_{ion} is the mobility of positive air ions (1.4 $cm^2\ V^{-1}\ s^{-1}$), E is the mean value of the electric field intensity, e is the elementary unit of charge (1.6×10^{-19} C), and A is the surface area of the rod. The average charge number per particle size, n_{dp}, obtained from the corona charger is estimated by using the following equation:

$$n_{d_p} = \frac{I_{d_p}}{P \cdot N_{1,d_p} \cdot e \cdot Q} \tag{2}$$

where I_{dp} is the current due to the charged aerosols exiting the charger, P is the penetration, Q is the air flow rate, and $N_{1,dp}$ is the number concentration of aerosol particles of size d_p entering the charger (# cm^{-3}).

Theoretically, n_{dp} can be calculated by using the following equation:

$$n_{d_p} = \frac{d_P k_B T}{2K_E e^2} \ln\left[1 + \frac{\pi K_E d_P \bar{c}_{ion} e^2 N_{ion} t}{2k_B T}\right] + \left(\frac{3\varepsilon}{\varepsilon + 2}\right)\left(\frac{E d_p{}^2}{4K_E e}\right)\left(\frac{\pi K_E e Z_{ion} N_{ion} t}{1 + \pi K_E e Z_{ion} N_{ion} t}\right) \tag{3}$$

where k_B is the Boltzmann constant, K_E is the electrostatic constant of proportionality (9×10^9 N m^2 C^{-2}), $\bar{c}_{ion}$ is the mean thermal speed of an air ion (2.4×10^2 m s^{-1}), t is the charging time, ε is the relative permittivity of the particle, and Z_{ion} is the mobility of the ion (approximately 1.5×10^{-4} $m^2\ V^{-1}\ s^{-1}$) (Hinds, 1999).

The wall loss of particles of size d_p, $WL_{charger,dp}$ is defined as the ratio of the outlet concentration of particles to the inlet concentration of particles through the charger:

$$WL_{charger,d_p} = \frac{N_{1,d_p} - N_{2,d_p}}{N_{1,d_p}} \tag{4}$$

where $N_{2,dp}$ is the concentration of aerosol particles exiting the charger.

The cutoff characteristic of each impactor stage is expressed as the Stokes number.

$$Stk = \frac{\tau U}{W/2} = \frac{\rho_{H_2O} d_A{}^2 U C_c}{9\mu W} \tag{5}$$

where τ is the relaxation time, U is the jet velocity, ρ_{H_2O} is the density of water (= 1000 kg m^{-3}), W is the nozzle diameter, and d_A is the aerodynamic diameter of a particle. The dynamic viscosity of air, μ (kg m^{-1} s^{-1}) and the slip correction factor, C_c, are calculated by using:

$$\mu = 1.8 \times 10^{-5} \left(\frac{T_{down}}{T_{up}}\right)^{3/2} \frac{T_{up} + 120}{T_{down} + 120} \tag{6}$$

$$C_c = 1 + \frac{1}{1000 p_{down} d_A}\left[15.6 + 7\exp\left(-59 p_{down} d_A\right)\right] \quad (7)$$

where T_{up} and T_{down} represent temperatures (Kelvin) at the upstream and downstream of each impactor stage, respectively, and p_{down} (Pa) represents the pressure at the downstream of each impactor stage. In Eq. (7), the unit of d_A is meter. The following equation is obtained from the energy conservation:

$$T_{down} = T_{up} - \frac{U^2}{2c_p} \quad (8)$$

The specific heat under constant pressure, c_p is defined as

$$c_p = \frac{\gamma R_u}{(\gamma - 1) M} \quad (9)$$

where R_u is the universal gas constant (J K^{-1} $kmol^{-1}$), M is the molar weight of air (kg $kmol^{-1}$), and γ is the specific heat ratio.

Each stage of the impactor is characterized by its cutoff diameter and particle collection efficiency curve. In practice, due to the flow pattern at the nozzle outlet, the collection efficiency curve is typically "S"-shaped. The collection efficiency, η, is expressed as

$$\eta = \frac{1}{1 + \left(\frac{d_{50}}{d_A}\right)^x} \quad (10)$$

where χ is the steepness of the collection efficiency curve (Dzubay and Hasan, 1990; Winklmayr *et al.*, 1990; Park *et al.*, 2009; Jarvinen *et al.*, 2014). The cutoff diameter of each stage, d_{50} is defined as the aerodynamic diameter having 50% collection efficiency. For a circular nozzle, Eq. (5) can be rearranged to give the cutoff diameter in terms of Stk_{50}, which is the Stokes number at 50% collection efficiency, as follows:

$$d_{50} = \sqrt{\frac{9\mu W Stk_{50}}{\rho_{H_2O} U C_c}} \quad (11)$$

The relation between the jet velocity and pressure is expressed as

$$p_{down} = p_{up} - \frac{1}{2}\rho_{down} U^2 \quad (12)$$

where p_{up} and p_{down} represent the pressures at the upstream and downstream of each impactor stage, respectively. The density at the downstream of each impactor stage, p_{down} is

$$\rho_{down} = \rho_{up}\left(p_{down} / p_{up}\right)^{1/\gamma} \quad (13)$$

where p_{up} is the density at the upstream.

In this study, by assuming $Stk_{50}^{1/2}$ as 0.49 (Hinds, 1999) and assuming arbitrary values of the nozzle diameter and the number of nozzles for each impactor stage, the cutoff diameter for each impactor stage can be calculated by using the following procedure. For this, the pressures at the upstream and downstream are measured for each stage and used to calculate the density at the downstream with Eq. (13). Then, the jet velocity is obtained by using Eq. (12), and the cutoff diameter is determined by using Eq. (11). The procedure is repeated until the calculated d_{50} is nearly equal to the designed d_{50} for each impactor stage. Table 1 summarizes the design specifications of the ECI.

DATA PROCESSING

A data inversion method is needed to convert the electrical current data of the charged particles into a size distribution. In this paper, the method proposed by Park *et al.* (2007) is modified and used. While it is assumed in Park *et al.* (2007) that the size distribution of incoming particles follows a unimodal log normal distribution, in this study the distribution of particles captured at each stage (including Faraday cage) is assumed as a unimodal log normal distribution so that the incoming particles may follow any size distribution.

A residual function ξ is defined as

$$\xi^2\left(N_{t,i}, d_{g,i}, \sigma_{g,i}\right) = \left(I_{measured,i} - I_{theoretical,i}\right)^2 \quad i = 1,2,3,4,5 \quad (14)$$

where the subscript i represents each stage (the subscript 5 represents the Faraday cage stage), $N_{t,i}$ is the total number concentration of particles captured at the i^{th} stage, $d_{g,i}$ and $\sigma_{g,i}$ are the geometric mean diameter and geometric

Table 1. Specifications of each stage of ECI.

Stage	Designed D_{50} (nm)	Designed $Stk_{50}^{1/2}$	Re-Designed D_{50} (nm)	Nozzle diameter (mm)	Nozzle number	Inlet pressure (kPa)	Outlet pressure (kPa)	Jet velocity (m s^{-1})
Pre	250	0.49	203	0.25	58	101.33	91.72	130.82
1	150	0.49	129	0.4	11	91.72	61.27	268.95
2	94	0.49	70.6	0.3	30	61.27	37.01	287.42
3	54	0.49	53.7	0.3	69	37.01	25.81	222.0
4	30	0.49	39.3	0.3	52	25.81	19.60	182.63

standard deviation of particles captured at the i^{th} impactor stage, respectively, and $I_{measured,\,i}$ is the current measured at the i^{th} stage.

The theoretical current, $I_{theoretical,i}$ at the i^{th} stage is derived by

$$I_{theoretical,i} = Qe \sum_{j=min}^{max} \left\{ P \cdot n\left(d_{p,j}\right) \right\} \times N_i\left(d_{p,j}\right) \quad i = 1,2,3,4,5 \tag{15}$$

where $d_{p,j}$ is the diameter of j^{th} sized particle. $P \cdot n(d_{p,j})$ can be expressed by the following equation,

$$P \cdot n\left(d_{p,j}\right) = 58.01 \times d_{p,j}^{\,1.3437} \quad (dimensionless) \tag{16}$$

where the unit of $d_{p,j}$ is μm.

Assuming a log-normal distribution, the size distribution of aerosol particles captured at each stage can be obtained by

$$N_i\left(d_{p,j}\right) = N_{t,i} \frac{\left(\ln d_{p,j+1} - \ln d_{p,j}\right)}{\sqrt{2\pi}\ln\sigma_{g,i}} \exp\left[\frac{\left(\ln d_{p,j} - \ln d_{g,i}\right)^2}{2ln^2\sigma_{g,i}}\right]$$

$$i = 1,2,3,4,5 \tag{17}$$

where $N_{t,i}$ is the number concentration of particles captured at the i^{th} impactor stage.

After $I_{theoretical,i}$ and $I_{measured,i}$ are inserted into Eq. (14), the residual function at each stage is minimized so that optimal values of $N_{t,i}$, $d_{g,i}$ and $\sigma_{g,i}$ can be determined. Then the number based size distribution of incoming aerosols $N(d_p)$ can be obtained from the following equation,

$$N\left(d_p\right) = \frac{\sum N_i\left(d_{p,j}\right)}{\sum E_i\left(d_{p,j}\right)} \tag{18}$$

where the modified collection efficiency suggested by Dong *et al.* (2004) and Marjamäki *et al.* (2005) is as follows;

$$E_i\left(d_{p,j}\right) = \eta_i\left(d_{p,j}\right) \times \prod_{1}^{i=5}\left[1 - \eta_{i-1}\left(d_{p,j}\right)\right] \quad i = 1,2,3,4,5 \tag{19}$$

$$E_0(d_{p,j}) = \eta_0\,(d_{p,j}) \tag{20}$$

where the collection efficiency of particles at the i^{th} stage, η_i, is defined as in Eq. (21). The subscript 0 represents the precut stage.

EXPERIMENTS

Particle Charge Number

The electrical characteristics of the wire-to-rod type corona charger were tested. The corona currents (I_C) of the charger according to various applied voltages (V) were measured by using a multimeter (METRAHIT X-TRA, Gossen Metrawatt, UK).

To evaluate the particle loss and charging characteristics of the charger, an experimental setup was constructed, as shown in Fig. 1, and test aerosol particles were generated. Compressed air was used as the carrier gas, after oil droplets, moisture, and contamination particles were removed by a clean air supply, which consisted of an oil trap, diffusion dryer, and HEPA filter. A metal nanoparticle generator (EP-NGS20, EcoPictures, Korea) was used to generate monodisperse Ag nanoparticles with diameters in the range

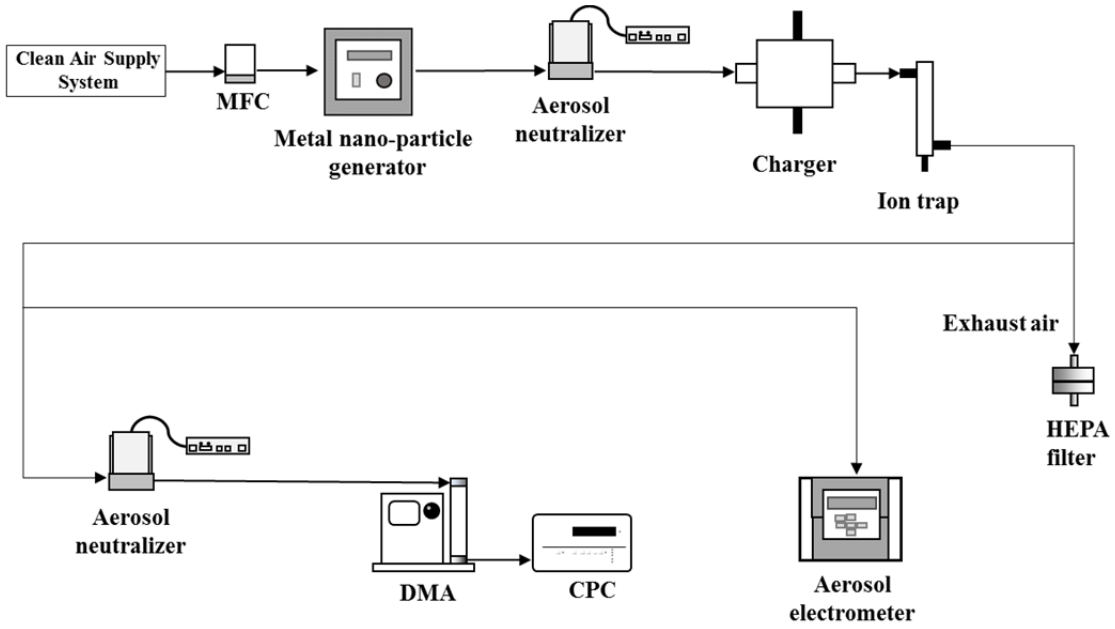

Fig. 1. Experimental setup for evaluating particle charging characteristics.

of 10–100 nm. The concentration range was 10^6–10^7 # cm^{-3}. In the nanoparticle generator, Ag nanoparticles are generated by evaporation/condensation using a small ceramic heater with a local heating area (Jung *et al.*, 2006). The size distribution of aerosolized Ag nanoparticles is shown in Supplemental Information.

The particles were carried by the air at a flow rate of 10 L min^{-1}. Then, a soft X-ray type aerosol neutralizer (4530, HCT, Korea) was used to make the particles have Boltzmann equilibrium charge distribution. The particles were charged by passing them through the charger. The free ions leaving the charger were removed by using an ion trap. The voltage applied to the ion trap was 20 V. Details of the ion trap are explained in Supplemental Information. Then, the geometric mean diameter and total number concentration of the particles were measured using SMPS. An aerosol electrometer (AE, 3068B, TSI, USA) was used in parallel to measure the current of the charged particles.

Particle Collection Efficiency

To evaluate the collection efficiency of each impactor stage, an experimental setup was constructed, as shown in Fig. 2. Polystyrene latex (PSL) particles were generated from an atomizer (9302, TSI, USA), which produced an aerosol of small particles by removing the larger spray droplets by impaction within the device. PSL particles of various sizes (20–370 nm) were tested. The airflow rate to the atomizer was maintained at 2 L min^{-1}.

In order to supply monodisperse PSL particles, the particles passing through the neutralizer were classified by a differential mobility analyzer (DMA, 3081, TSI, USA). The size distributions of DMA-classified PSL particles are shown in Supplemental Information. The particle flow rate exhausted from the DMA was 0.3 L min^{-1}. Once the single positively charged particles of a certain diameter were classified by the DMA, the particles were exposed to another neutralizer. Next, the charge-redistributed particles were mixed with clean air at a rate of 10 L min^{-1}. In order to charge the particles that were mixed with clean air, they were passed through the aerosol charger. The free ions leaving the charger were removed using an ion trap. The particles entering the ECI, and the currents carried by the charged particles were measured using a 6-channel lab-made electrometer.

The collection efficiency of the particles at the i^{th} stage was obtained by using Eq. (21)

$$\eta_i = \frac{I_{measured,i}}{\sum I_{measured,i}} \qquad i = 0,1,2,3,4,5 \tag{21}$$

where $I_{measured,\,i}$ is the current measured at the i^{th} stage. To measure the charge carried by the particles, we used a lab-made electrometer that can measure 1 fA using a three stage amplifier circuit. The performance of the lab-made electrometer was compared with that of a commercial electrometer (Keithly 6517B) for particle sizes in the range of 30–2500 nm, and number concentration in the range of

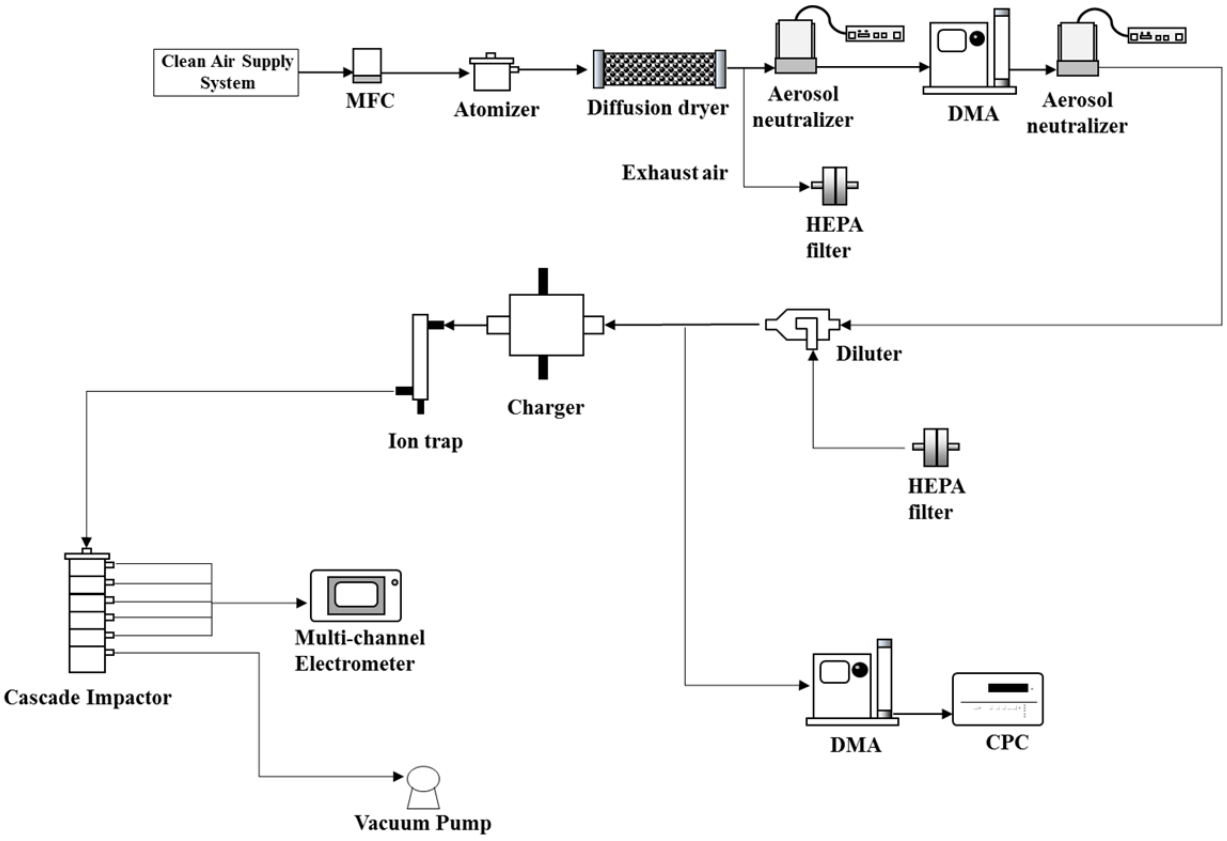

Fig. 2. Experimental setup for evaluating the collection efficiency of each stage.

10–1,000 # cm^{-3}. The circuit diagram and results of the performance test of the electrometer are shown in the supplemental information.

Particle Size Distribution

After evaluating the collection efficiency of each impactor stage, the size distribution of the test particles was estimated by the data inversion algorithm, and it was compared with the data measured by the SMPS. Fig. 3 shows the schematic for the comparison test in the laboratory. In the test, a tube furnace (GTF12/25/364, Lenton Furnaces, UK) was used to generate polydisperse sodium chloride (NaCl) particles. After dilution with air cleaned by a HEPA filter, the size distribution was measured using the SMPS. Simultaneously, the size distribution was also calculated using the data inversion algorithm from the measured currents

RESULTS AND DISCUSSION

Particle Charge Number

Before the particle charging characteristics of the charger were evaluated with the setup shown in Fig. 1, the current-voltage characteristics were obtained. The results are shown in Fig. 4. The corona starting voltage was about 3 kV. For the applied voltage of 4 kV, the ion concentration, N_{ion}, was estimated as 3.31×10^9 # cm^{-13} (see Eq. (1)).

Fig. 5 shows the measured and theoretically calculated charge numbers for different particle sizes. Overall, the theoretical charge numbers are slightly higher than the measured ones. For example, for a 10 nm-diameter particle, the theoretical and measured charge numbers are 0.23 and 0.18, respectively. This could be because the theory used in this study is based on a single particle interacting with all the surrounding ions. Therefore, the number of ions participating in particle charging will be higher in theory than in the experiment.

Fig. 6 shows the results of penetration and $P{\cdot}n$ value versus particle size. The particle penetration (P) was obtained by measuring the number concentrations at the upstream and downstream of the charger. The $P{\cdot}n$ value varied from 0.155 to 2.543 when the particle size varied from 10 nm to 100 nm, while the particle penetration varied slightly between 0.49 and 0.68 (average = 0.58).

Particle Collection Efficiency

Using the schematic shown in Fig. 2, the collection efficiency curve of each impactor stage was experimentally obtained, and the results are shown in Fig. 7. Different PSL sizes were used: 370, 300, 260, 200, 160, 140, 100, 90, 80, 60, 30, and 20 nm. Once the particles were generated, the current of each stage was measured and then used to calculate the collection efficiency by using Eq. (22). Table 1 shows that the cutoff diameters were originally 250, 150,

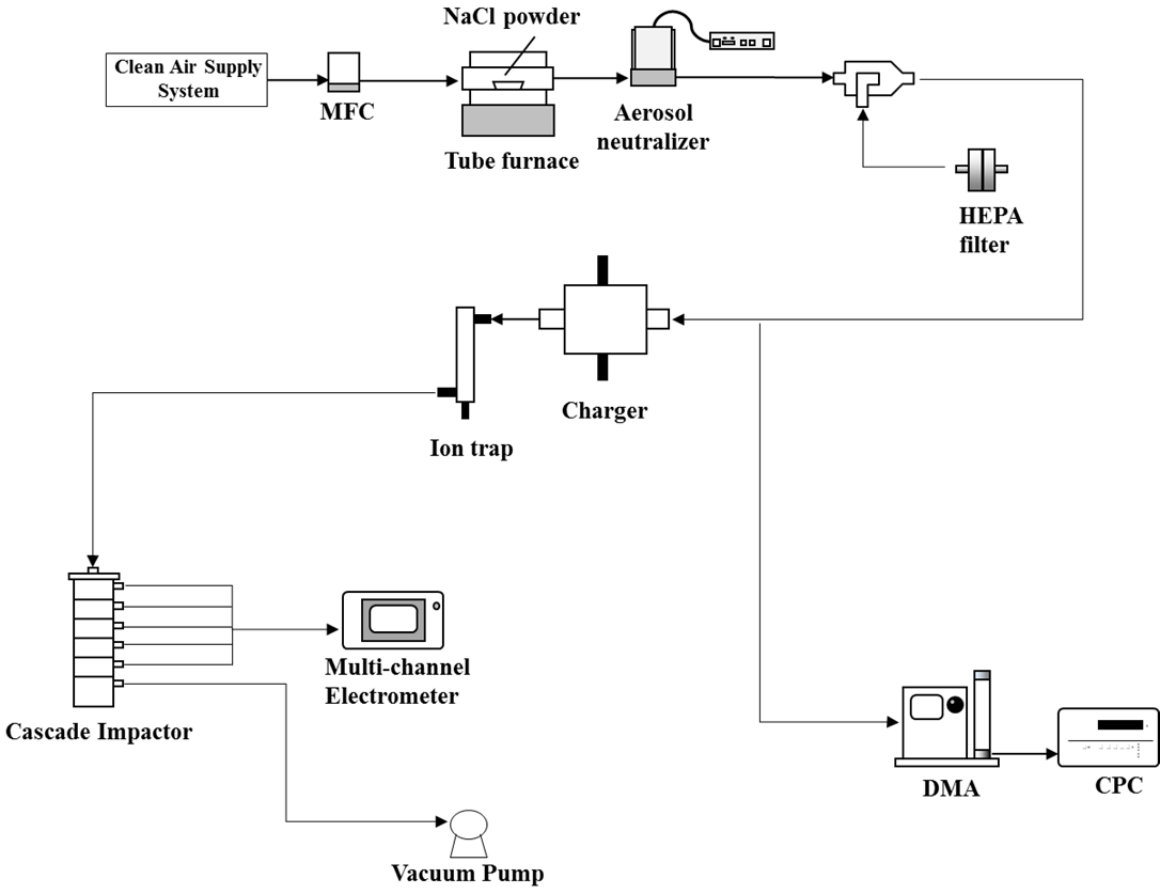

Fig. 3. Experimental setup for comparing ECI data with SMPS data.

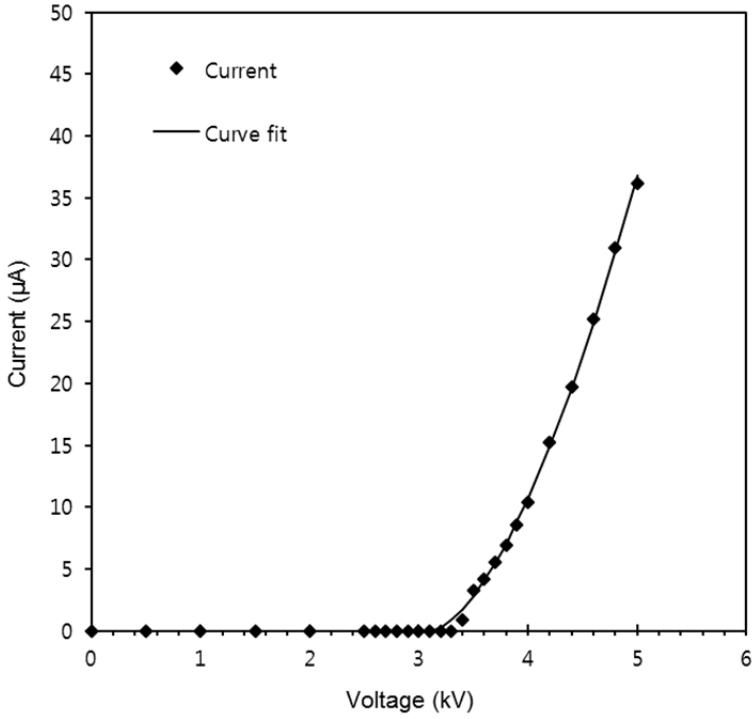

Fig. 4. Current-voltage characteristics of the charger.

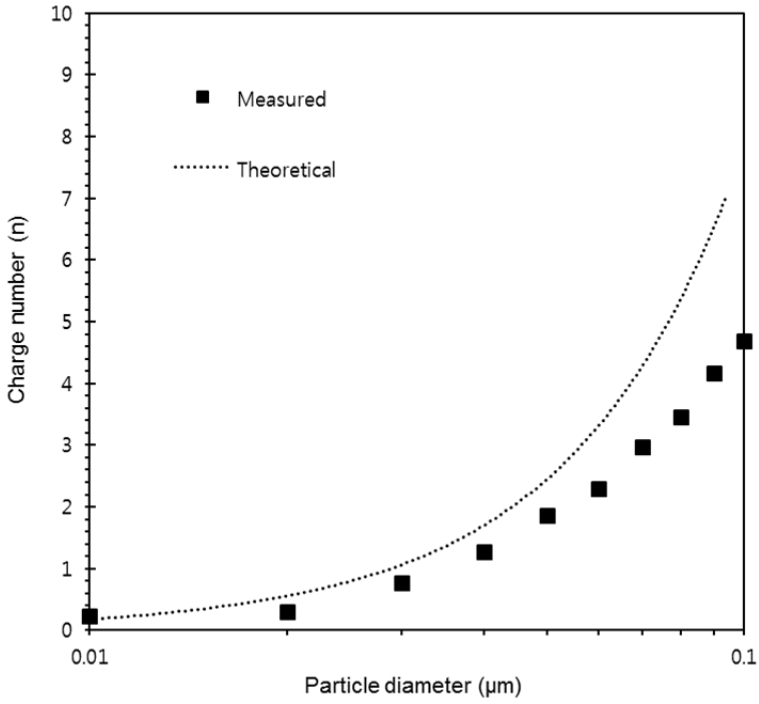

Fig. 5. Calculated charge number versus particle size.

94, 54, and 30 nm (design values) but were changed to 203, 129, 71, 54, and 39 nm (re-design values) after selection of nozzle size and number in each impactor stage. The calculated upstream and downstream pressures as well as jet velocity in each stage are also shown in Table 1. Table 2 shows that the measured pressure data were in good agreement with the theoretically calculated ones shown in Table 1. Table 2 also shows that the experimentally determined cutoff diameters were 200, 110, 83, 59, and 29 nm and were close to the re-designed values of 203, 129, 71, 54, and 39 nm. In Table 2, the experimental value of $Stk_{50}^{1/2}$ in each stage was determined from the jet velocity for given nozzle diameter and experimentally determined cutoff diameter. It was found that the value of $Stk_{50}^{1/2}$ in

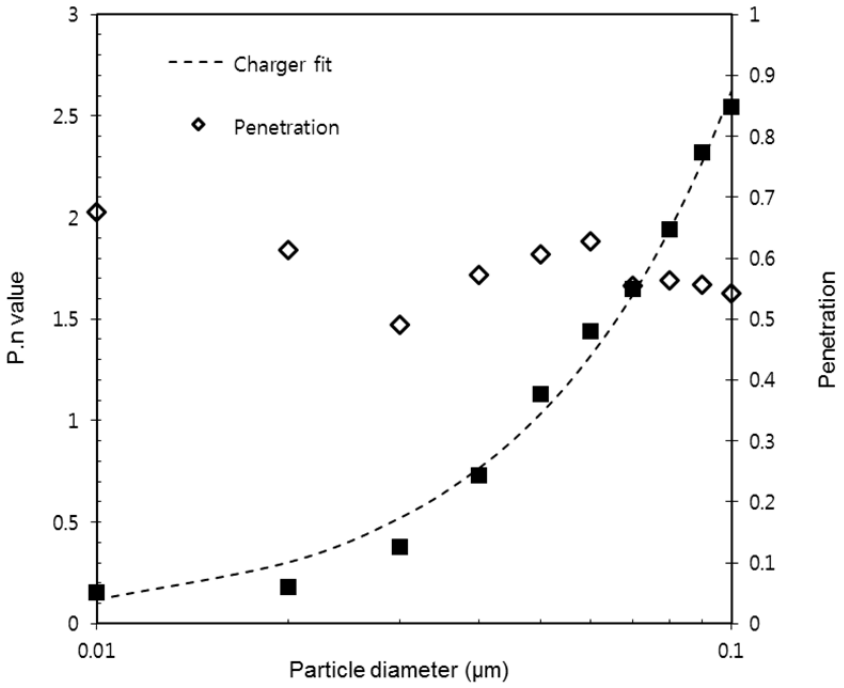

Fig. 6. Penetration and P.n value versus particle size.

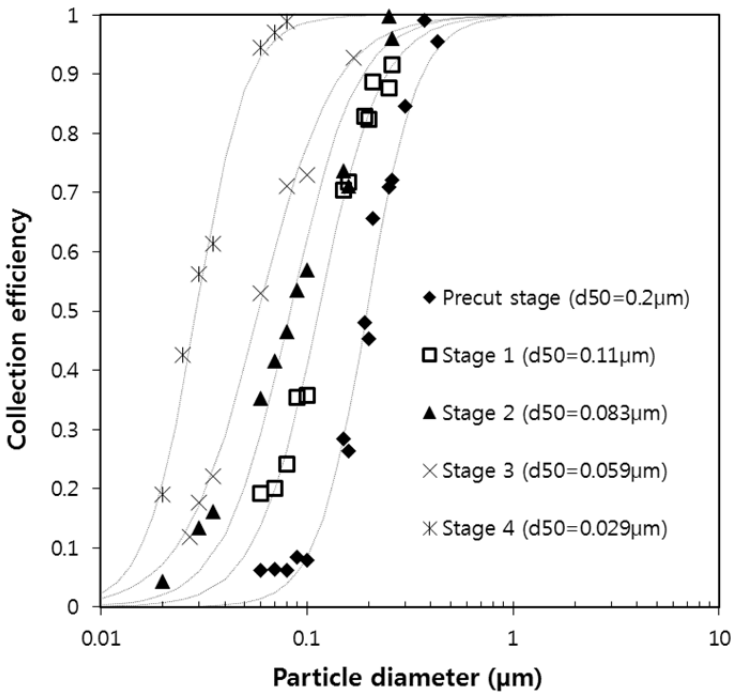

Fig. 7. Collection efficiency of each stage.

Table 2. Experimental results of each stage of ECI.

Stage	Re-Designed D_{50} (nm)	Experimental D_{50} (nm)	Inlet pressure (kPa)	Outlet pressure (kPa)	Experimental $Stk_{50}^{1/2}$	Slope of the efficiency
Pre	203	200	100.67	91.05	0.48	3.55
1	129	110	91.05	60.55	0.459	2.86
2	70.6	83	60.55	46.89	0.434	2.70
3	53.7	59	46.89	33.18	0.462	2.36
4	39.3	29	33.18	21.10	0.452	3.54

each impactor stage was close to the designed value of 0.49. The values of the efficiency curve slope, which represents the performance of an impactor, were 3.55, 2.86, 2.70, 2.36, and 3.54 for the precut stages 1, 2, 3, and 4, respectively. Fig. 8 shows the modified collection efficiency for each stage.

Particle Size Distribution

Fig. 9(a) shows the size distribution of NaCl particles captured at each stage, $N_i(d_{p,j})$. The measured current values were 1460, 2021, 302, 2215, and 104 fA, respectively, for Stages 1, 2, 3, 4, and 5 (Faraday cage). Each measured current was converted into a number-based size distribution of particles by the data inversion algorithm. The total number concentration values were 1.15×10^4, 3.04×10^4, 0.88×10^4, 9.21×10^4, and 0.75×10^4 # cm^{-3}, respectively, for Stages 1, 2, 3, 4, and 5 (Faraday cage). The geometric mean diameters were 136, 82, 52, 38, and 26 nm and the geometric standard deviations were 1.55, 1.61, 1.52, 1.64, and 1.65, respectively, for Stages 1, 2, 3, 4, and 5 (Faraday cage).

Fig. 9(b) was obtained using Eq. (18) after the five individual size distributions shown in Fig. 9(a) were determined. In Fig. 9, the particle diameter in the x-axis was expressed as aerodynamic diameter. The mobility diameter of SMPS data was changed to the aerodynamic diameter using the following equation;

$$\rho_{eff} = \rho_{H_2O} \frac{d_a^{\,2} C_a}{d_m^{\,2} C_m} \tag{22}$$

where ρ_{H_2O} is the density of water (1.0 g cm^{-3}), d_a and d_m are the aerodynamic and mobility diameters, respectively; C_a and C_m are the slip correction factors for the aerodynamic diameter and mobility diameter, respectively. The effective density of NaCl particles was obtained with the following two equations:

$$\rho_{eff} = \rho_p \left[\frac{d_{ve}}{d_m} \right]^3 \tag{23}$$

$$\frac{d_{ve}}{C_{ve}} = \frac{d_m}{\chi C_m} \tag{24}$$

where ρ_p is the particle density, d_{ve} is the volume equivalent diameter, C_{ve} is the slip correction factor for the volume equivalent diameter, and χ is the dynamic shape factor. The NaCl particles are cubic ($\chi = 1.08$) and have a density of 2.163 g cm^{-3}. Therefore, the effective density of NaCl particles can be calculated.

In Fig. 9(b), the total concentration, geometric mean diameter, and geometric standard deviation of the ECI data were 1.65×10^5 # cm^{-3}, 59.6 nm, and 2.16, respectively. For the comparison test, the size distribution of NaCl particles was measured by using the SMPS. The SMPS data were the total concentration of 1.07×10^5 # cm^{-3}, the geometric mean diameter of 56.4 nm, and the geometric standard deviation of 1.55. Therefore, the ECI data obtained from the data inversion algorithm with current measurement match well with the SMPS data, even when there is a slight difference in the geometric standard deviation. In addition, the ECI data shows a higher number concentration than the SMPS data for the particles larger than 88 nm.

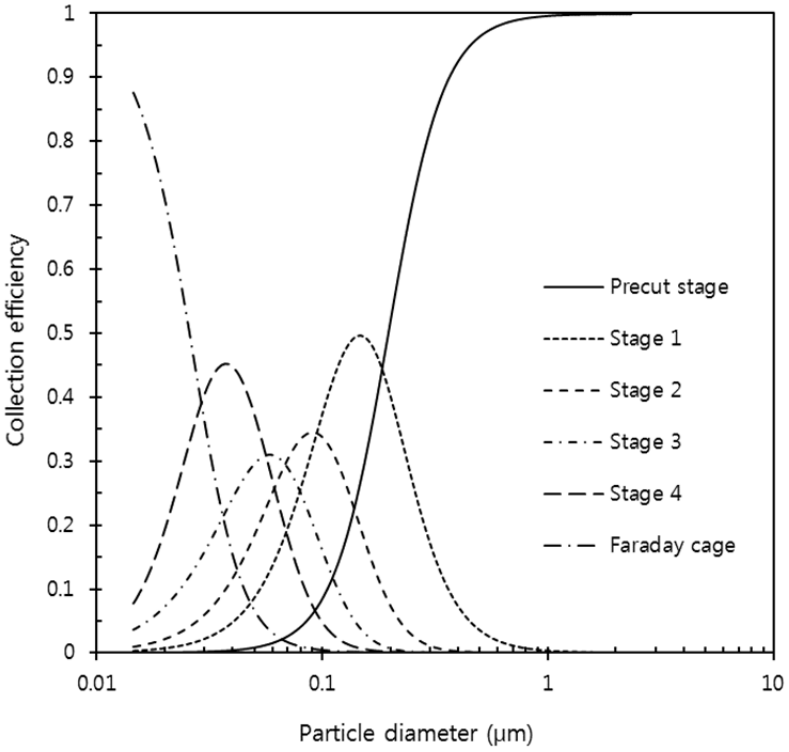

Fig. 8. Modified collection efficiency for each stage.

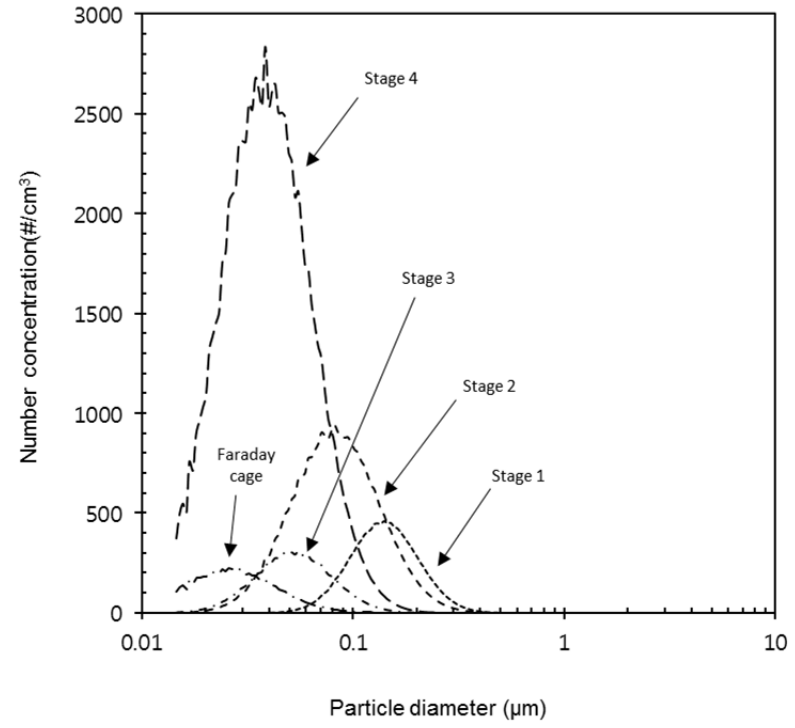

(a)

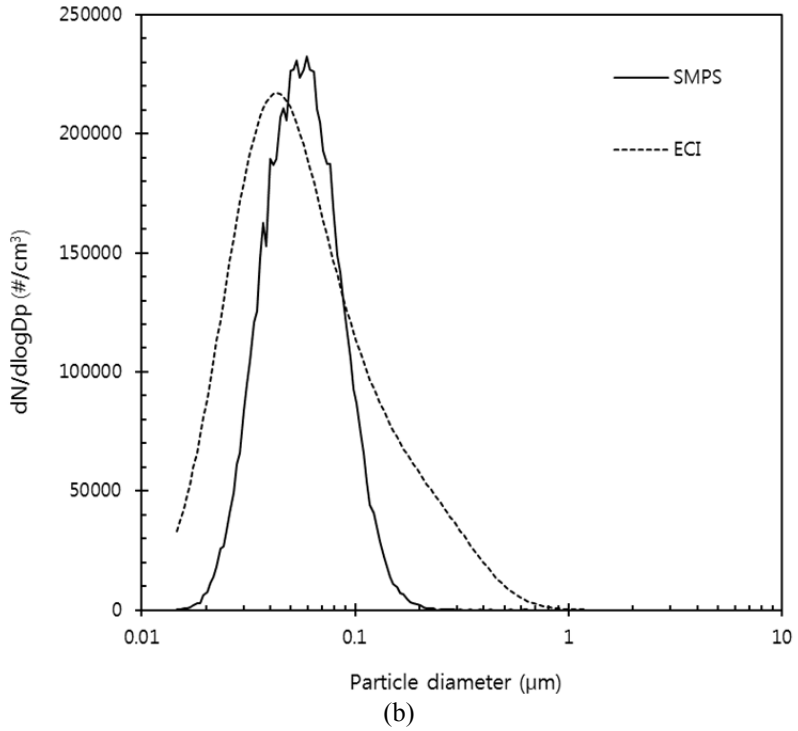

(b)

Fig. 9. (a) Particle size distribution of each stage (NaCl particles) and (b) Particle size distributions by SMPS and ECI (NaCl particles).

The ECI was also tested in an outdoor environment, and the result is shown in Fig. 10. Since the effective density of ambient particles was not known, it was assumed that the effective density of ambient particles was the unity in Fig. 10. While the SMPS data show a total concentration of 1.76×10^4 # cm^{-3}, geometric mean diameter of 71 nm, and geometric standard deviation of 2.36, the ECI data show a total concentration, geometric mean diameter, and geometric standard deviation of 2.22×10^4 # cm^{-3}, 69 nm, and 2.54, respectively. From Figs. 9 and 10, it can be seen that the ECI data are in agreement with the SMPS data.

In this study, the performance of the ECI was also tested

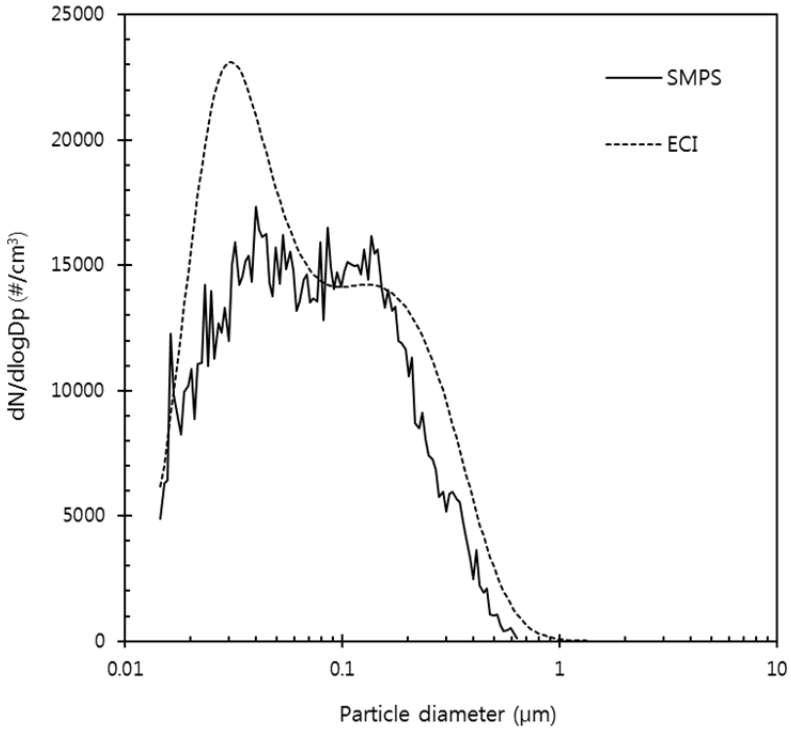

Fig. 10. Particle size distributions by SMPS and ECI (Ambient particles).

for particles having an assumed size distribution. Two cases were considered: (1) constant number concentration for particle sizes of 26–360 nm (total concentration = 2.83 × 10^4 # cm^{-3}) and (2) bimodal lognormal distribution. Since this test was carried out without any experiment, Eq. (14) was modified as follows:

$$\xi^2\left(N_{t,i}, d_{g,i}, \sigma_{g,i}\right) = \left(I_{assumed,i} - I_{theoretical,i}\right)^2 \quad i = 1,2,3,4,5 \tag{25}$$

where

$$I_{assumed,i} = Qe\sum_{j=min}^{max}\left\{P\cdot n\left(d_{p,j}\right)\right\}\times N_{assumed}\left(d_{p,j}\right)\times E_i\left(d_{p,j}\right)$$
$$i = 1,2,3,4,5 \tag{26}$$

For Case 1, the data inversion algorithm was performed using the currents obtained by Eq. (26). Fig. 11 shows that the ECI result was similar to the assumed one. The total concentration obtained by the ECI was 2.76 × 10^4 # cm^{-3}, which was in good agreement with the assumed concentration of 2.83 × 10^4 # cm^{-3}.

For Case 2, it was assumed that the particles had a bimodal lognormal distribution, which was the summation of two individual unimodal lognormal distributions: the number concentrations of 1 × 10^4 # cm^{-3} and 1.2 × 10^4 # cm^{-3}, the geometric mean diameters of 148 nm and 40 nm, the geometric standard deviations of 1.65 and 1.6, respectively, for the right and left distributions. Fig. 12 shows that the size distribution obtained with the ECI was also a bimodal distribution. The geometric mean diameters of the ECI were 140 nm and 41 nm, respectively, for the right and left distributions, which were in good agreement with the assumed ones. The total concentration of 2.18 × 10^4 # cm^{-3} obtained with the ECI was very close to the assumed value of 2.19 × 10^4 # cm^{-3}.

CONCLUSIONS

In this study, a laboratory-made electrical cascade impactor was designed to measure the real-time size distribution of aerosols with a 200-nm precut. The experimentally determined cut-off diameters were 200, 110, 83, 59, and 29 nm, which were in agreement with the calculated values. In the data inversion algorithm that was developed, the distribution of particles captured at each stage (including the Faraday cage) was assumed to be a unimodal lognormal distribution, meaning that the incoming particles may follow any size distribution.

In the performance test in both the laboratory and the field, the ECI data matched well with the SMPS data. The performance of the ECI was also tested for particles having an assumed size distribution. For the two cases that were considered, (1) a constant number concentration for any particle size and (2) a bimodal lognormal distribution, the ECI data were in good agreement with the assumed data.

ACKNOWLEDGMENTS

This research was supported by the Korean Ministry of Environment (MOE) as the Technologies for Responding to Atmospheric Environment Policies Program.

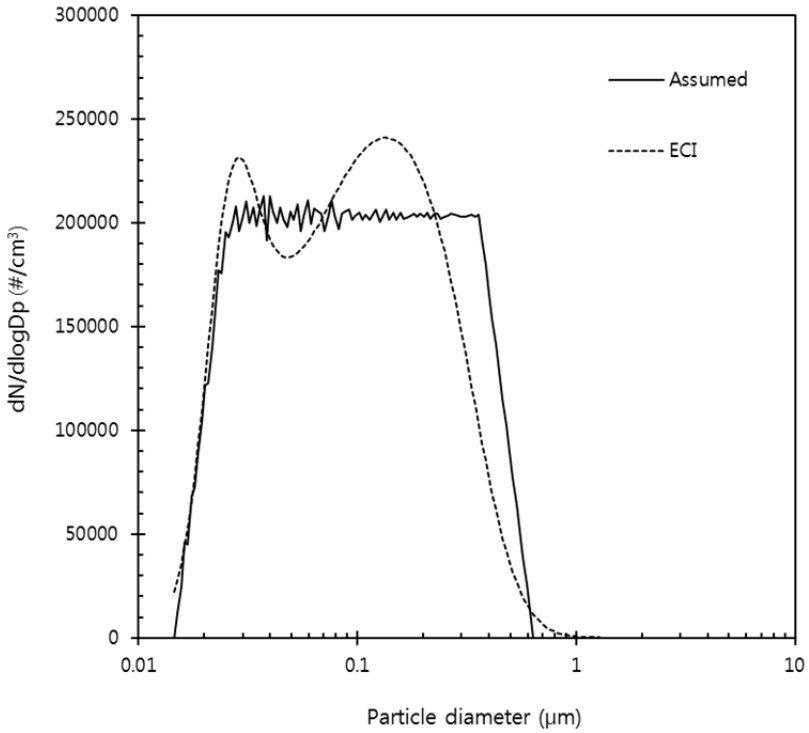

Fig. 11. Particle size distributions by assumed particles and ECI (constant number concentration).

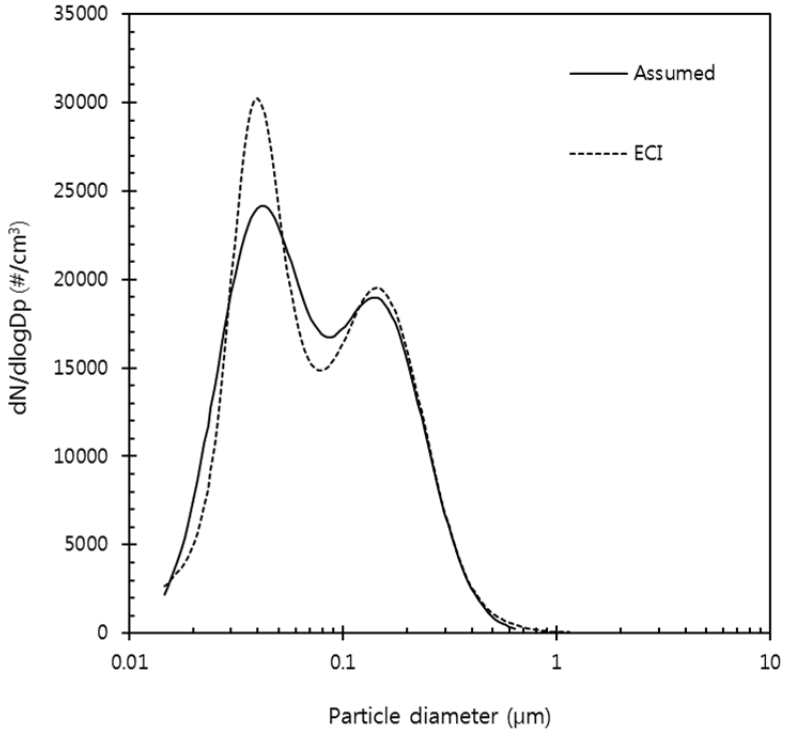

Fig. 12. Particle size distributions by assumed particles and ECI (bimodal log normal distribution).

SUPPLEMENTARY MATERIAL

Supplementary data associated with this article can be found in the online version at http://www.aaqr.org.

REFERENCES

Alonso, M., Martin, M.I. and Alguacil, F.J. (2006). The measurement of charging efficiencies and losses of aerosol nanoparticles in a corona charger. *J. Electrostat.*

64: 203–214.

Domat, M., Kruis, F.E. and Fernandez-Diaz, J.M. (2014). Investigations of the effect of electrode gap on the performance of a corona charger having separated corona and charging zones. *J. Aerosol Sci.* 68: 1–13.

Dong, Y., Hays, M.D., Smith, N.D. and Kinsey, J.S. (2004). Inverting cascade impactor data for size-resolved characterization of fine particulate source emissions. *J. Aerosol Sci.* 35: 1497–1512.

Dzubay, T.G. and Hasan, H. (1990). Fitting multimodal lognormal size distributions to cascade impactor data. *Aerosol Sci. and Tech.* 13: 144–150.

Hinds, W.C. (1999). *Aerosol technology: Properties, behavior, measurement of airborne particles*, John Wiley & Sons.

Järvinen, A., Aitomaa, M., Rostedt, A., Keskinen, J. and Yli-Ojanperä, J. (2014). Calibration of the new electrical low pressure impactor (ELPI+). *J. Aerosol Sci.* 69: 150–159.

Jiang, P., Yang, L., Chen, X., Gao., Y., Li, Y., Zhang, J., Zhao, T., Yu, H. and Wang, W. (2018). Impact of dust storms on NPAHs and OPAHs in $PM_{2.5}$ in Jinan, China, in spring 2016: Concentrations, health risks, and sources. *Aerosol Air Qual. Res.* 18: 471–484.

Jung, J.H., Hyun, C.O., Hyung, S.N., Ji, J.H. and Kim, S.S. (2006). Metal nanoparticle generation using a small ceramic heater with a local heating area. *J. Aerosol Sci.* 37: 1662–1670.

Keskinen, J., Pietarinen, K. and Lehtimäki, M. (1992). Electrical low pressure impactor. *J. Aerosol Sci.* 23: 353–360.

Kleefsman, W.A. and van Gulijk, C. (2008). Robust method to compare aerosol chargers. *J. Aerosol Sci.* 39: 1–9.

Marjamäki, M., Keskinen, J., Chen, D.R. and Pui, D.Y.H. (2000). Performance evaluation of the electrical low-pressure impactor (ELPI). *J. Aerosol Sci.* 31: 249–261.

Marjamäki, M., Lemmetty, M. and Keskinen, J. (2005). ELPI response and data reduction I: Response functions. *Aerosol Sci. Technol.* 39: 575–582.

Li, N., Sioutas, C., Cho, A., Schmitz, D., Misra, C., Sempf, J., Wang, M., Oberley, T., Froines, J. and Nel, A. (2003). Ultrafine particulate pollutants induce oxidative stress and mitochondrial damage. *Environ Health Perspect.* 111: 455–460.

Li, N., Xia, T. and Nel A.E. (2008). The role of oxidative stress in ambient particulate matter-induced lung diseases and its implications in the toxicity of engineered nanoparticles. *Free Radical Biol. Med.* 44: 1689–1699.

Park, D., Kim, S., An, M. and Hwang, J. (2007). Real-time measurement of submicron aerosol particles having a log-normal size distribution by simultaneously using unipolar diffusion charger and unipolar field charger. *J. Aerosol Sci.* 38: 1240–1245.

Park, D., Choi, N.K., Lee, S.G. and Hwang, J. (2009). Real-time measurement of the size distribution of diesel exhaust particles using a portable 4-stage electrical low pressure impactor. *Part. Part. Syst. Char.* 26: 179–186.

Pope, C.A. and Dockery, D.W. (2006). Health effects of fine particulate air pollution: Lines that connect. *J. Air Waste Manage. Assoc.* 56: 709–742.

USEPA (2009). *Integrated science assessment for particulate matter.* US Environ. Prot. Agency Washington, DC.

Yli-Ojanperä, J., Kannosto, J., Marjamäki, M. and Keskinen, J. (2010). Improving the nanoparticle resolution of the ELPI. *Aerosol Air Qual. Res.* 10: 360–366.

Received for review, November 11, 2017
Revised, February 17, 2018
Accepted, February 25, 2018